Chemical sensing and imaging with metallic nanorods

Catherine J. Murphy,* Anand M. Gole, Simona E. Hunyadi, John W. Stone, Patrick N. Sisco, Alaaldin Alkilany, Brian E. Kinard and Patrick Hankins

Received (in Cambridge, UK) 20th July 2007, Accepted 26th September 2007
First published as an Advance Article on the web 23rd October 2007
DOI: 10.1039/b711069c

In this Feature Article, we examine recent advances in chemical analyte detection and optical imaging applications using gold and silver nanoparticles, with a primary focus on our own work. Noble metal nanoparticles have exciting physical and chemical properties that are entirely different from the bulk. For chemical sensing and imaging, the optical properties of metallic nanoparticles provide a wide range of opportunities, all of which ultimately arise from the collective oscillations of conduction band electrons (''plasmons'') in response to external electromagnetic radiation. Nanorods have multiple plasmon bands compared to nanospheres. We identify four optical sensing and imaging modalities for metallic nanoparticles: (1) aggregation-dependent shifts in plasmon frequency; (2) local refractive index-dependent shifts in plasmon frequency; (3) inelastic (surface-enhanced Raman) light scattering; and (4) elastic (Rayleigh) light scattering. The surface chemistry of the nanoparticles must be tunable to create chemical specificity, and is a key requirement for successful sensing and imaging platforms.

Department of Chemistry & Biochemistry and the W. M. Keck Laboratory for Bionanoparticle Technology Discovery and Development, University of South Carolina, Columbia, SC 29208, USA. E-mail: Murphy@mail.chem.sc.edu

Catherine J. Murphy

Catherine J. Murphy is the Guy F. Lipscomb Professor of Chemistry at the University of South Carolina. She received two BS degrees, one in chemistry and one in biochemistry, from the University of Illinois – Urbana-Champaign, in 1986. In 1990 she received her PhD in inorganic chemistry from the University of Wisconsin-Madison, under the direction of Arthur B. Ellis. From 1990–1993 she was an NSF and NIH postdoctoral fellow at the California Institute of Technology, with Jacqueline K. Barton. Since 1993 she has been a faculty member in the Department of Chemistry and Biochemistry at the University of South Carolina, winning numerous awards for both teaching and research. She and her research group have published over 120 papers in the areas of nanomaterials and biophysical chemistry. Her group has specialized in the synthesis, optical properties, chemical sensing and biological imaging applications of metallic nanomaterials; shape control of nanocrystals; optical probes of DNA structure and dynamics; nanocomposite materials; and inorganic coordination complexes for optical sensing. Murphy is a Senior Editor for the Journal of Physical Chemistry, a member of numerous Editorial Advisory Boards (including Chemical Communications), and is the Nanoscience Chair of the American Chemical Society's Division of Inorganic Chemistry for 2007–2008.

Introduction

Interest in ''finely-divided metals'' dates back to Roman times when gold was used for artistic coloration.[1,2] Today, we know that nanoscale metal particles are responsible for some of the beautiful colors in stained glass windows and other works of art.[1,2]

That gold appears red, or violet, or other colors that are *not* gold when prepared as a nanoscale material is one manifestation of the fact that nanoscale materials can possess distinct physical and chemical properties that are entirely different from their bulk counterparts.[3–5] If we classify materials according to their electronic properties and assign them either to metals, semiconductors, or insulators, then metals and semiconductors are by far more interesting to contemplate on the nanoscale. For semiconductors, quantum mechanical confinement of charge carriers occurs when the physical size of the crystallite approaches that of the Bohr radius of electron–hole pairs in the material – which is 1–10 nm for most semiconductors.[4] As a result, the optoelectronic properties of semiconductor nanoparticles vary with crystallite size in this regime.[4] This ability to engineer the nanocrystal bandgap by simply varying the size of the crystallite helps semiconductor nanoparticles (also called quantum dots) find applications in biomedicine as fluorescent labels, in electronics, solar cells *etc.*[4,6–8]

For metals, the situation is different. The mean free path of an electron in a metal at room temperature is approximately 10–100 nm.[9,10] Therefore, again, on similar length scales, interesting physical effects might be expected of metals. Even down to $\sim$5 nm, most metals can still be described as having a conduction band.[2,9,10] The bright colors in nanoscale noble metal particles are due to the collective oscillations of electrons in the conduction band that are excited by light of appropriate frequencies.[2,11–15] These oscillations are termed ''plasmons'' – or, more precisely for colloidal metal nanoparticles, localized

surface plasmon resonances (LSPRs).[11] The LSPR can be pictured as a "wave" of electrons sloshing over the surface of a metal nanoparticle. As a result, an enhanced electromagnetic field at and near the metal nanoparticle surface is set up, and this forms the basis for the surface-enhanced spectroscopies that will be discussed below.[11] The position of the plasmon band (extinction spectrum) is best measured on a conventional UV-visible spectrophotometer, and appears as a band with extremely high extinction coefficients (up to 10^{11} M^{-1} cm^{-1}).[11] It is important to realize, however, that this peak in the optical spectrum is not due to a simple ground state to excited state localized transition; and moreover, colloidal metal nanoparticles also scatter light very effectively, and their observed extinction spectra are really combinations of absorption and scattering.[11–15]

For a dilute solution of metallic small spherical particles, the resonance conditions to achieve absorption by light can be calculated using the analytical treatment of Maxwell's equations as demonstrated by Mie.[11,16] The resonance condition is met when the real part of the dielectric function of the metal equals the dielectric function of the surrounding medium in which the particles are dispersed. This condition also implies that the frequency of the plasmon band depends on the dielectric constant of its local medium.[11–17] In water, for example, it is well known that ~20 nm diameter spherical gold particles have their LSPR centered at ~520 nm, while silver nanospheres of the same size have their LSPR centered at ~420 nm. From further inspection of the parameters in Mie's equations, and others,[11–21] it can be deduced that the frequency of the plasmon band will differ from that of the simple isolated sphere if the nanoparticle is nonspherical in shape, and if it is close to other particles. The observations of multiple plasmon bands for anisotropic noble metal nanoparticles, and the known visible color changes that occur in solution when noble metal nanoparticles aggregate, clearly support these notions.[9–14,18–21] Scheme 1 shows the different parameters affecting the frequency of the LSPR band(s) for nanoparticles.[17,18]

The scattering component of the extinction spectra of noble metal nanoparticles is also sensitive to local environment. Just as the absorbed light of the LSPR is shifted by local refractive index, so is the color of scattered light.[22,23] This is best visualized in a simple darkfield optical microscope, in which white light impinges on the dispersed nanoparticle sample, and elastically scattered light is detected *via* the use of a darkfield objective (Fig. 1).

The large electromagnetic field produced by the plasmon(s) decays out perhaps ~10 nm at the most from the nanoparticle surface.[24] Any molecule that happens to be within this distance of the nanoparticle surface will experience these large fields. There are a number of "surface-enhanced" spectroscopies that result from this effect.[11,25] The principle effect that will be discussed here is surface-enhanced Raman spectroscopy (SERS), also known as surface-enhanced Raman scattering.[26] The Raman effect itself is a weak one: visible light that is not directly absorbed by the molecule of interest is only weakly

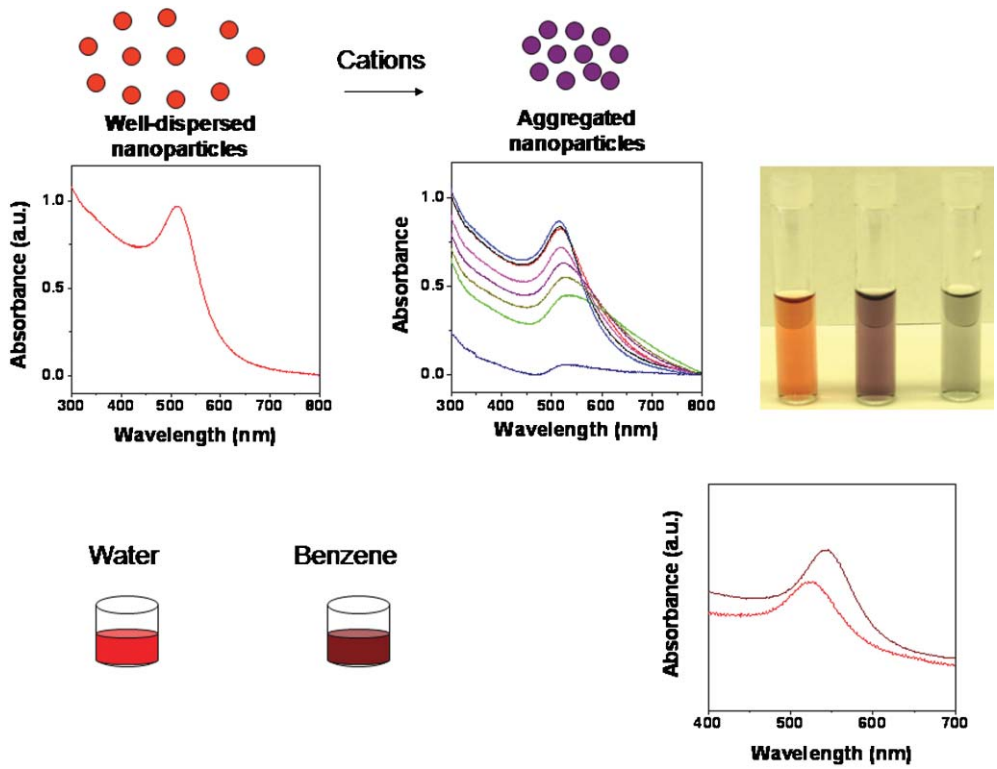

Scheme 1 The plasmon band position of noble metal nanoparticles can be used for chemical sensing. Top panel: Aggregation of noble metal nanoparticles red-shifts and broadens plasmon bands. For colloidal 4 nm gold nanospheres, this results in a visual color change from orange–red to purple or blue. The aggregation depicted here resulted from increased ionic strength in aqueous solution. Lower panel: The local refractive index of the medium shifts the position of the plasmon band.

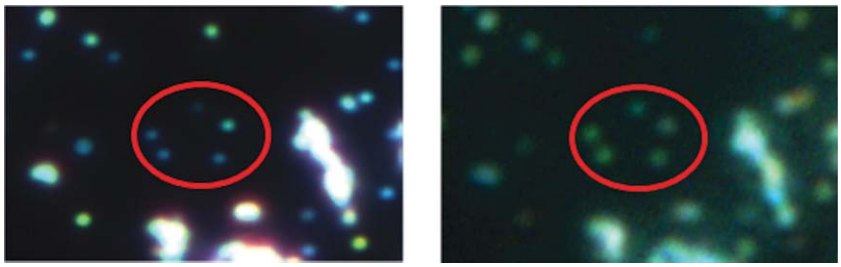

Fig. 1 Darkfield optical micrograph of light elastically scattered from silver nanoparticles, ~50 nm diameter. The field of view is approximately 1 mm. Left panel: Micrograph taken in air (refractive index 1). Right panel: Micrograph, same region, taken in mineral oil (refractive index ~1.5). The red-circled region highlights five spots that shift in scattered color from blues to greens.

inelastically scattered off the vibrations in the molecule. The fundamental selection rule for Raman spectroscopy is that the polarizability of the molecule must change during the course of the vibration. (In contrast, the fundamental selection rule for infrared spectroscopy is that the dipole moment of the molecule must change during the course of the vibration). The resulting Raman spectrum does provide a nice vibrational fingerprint of the molecule, and, unlike infrared spectroscopy, the O–H bond of water is only weakly Raman-active; but the required sample concentration to obtain a reasonable Raman spectrum is too high for this method to be generally useful for dilute (less than millimolar) concentrations. The intensity of Raman signals, however, depends on the fourth power of the local electric field. Molecules that are near a nanoscale metal surface not only experience this field, but also, through charge-transfer interactions with the metal surface itself, can undergo changes in polarizability that also increase its Raman signal - to the point of (near) single molecule detection.[25–28]

If we consider the light that is elastically scattered and inelastically scattered off noble metal nanoparticles, we can see the potential for imaging with nanoparticles using elastic light scattering, and the potential for chemical sensing with nanoparticles using SERS (Scheme 2).

For spherical nanoparticles, the plasmon oscillations are isotropic due to the spherical symmetry, but interesting differences emerge depending on the nanoparticle shape. For a nanorod, which we will define as a particle with a length/width ratio (also known as aspect ratio) between 1 and 20, the oscillations can now take place both along the width (transverse plasmon band) or along the length of the nanorod (longitudinal plasmon band).[9,29–31] Thus, two principle plasmon bands are observed in nanorods that are tunable with

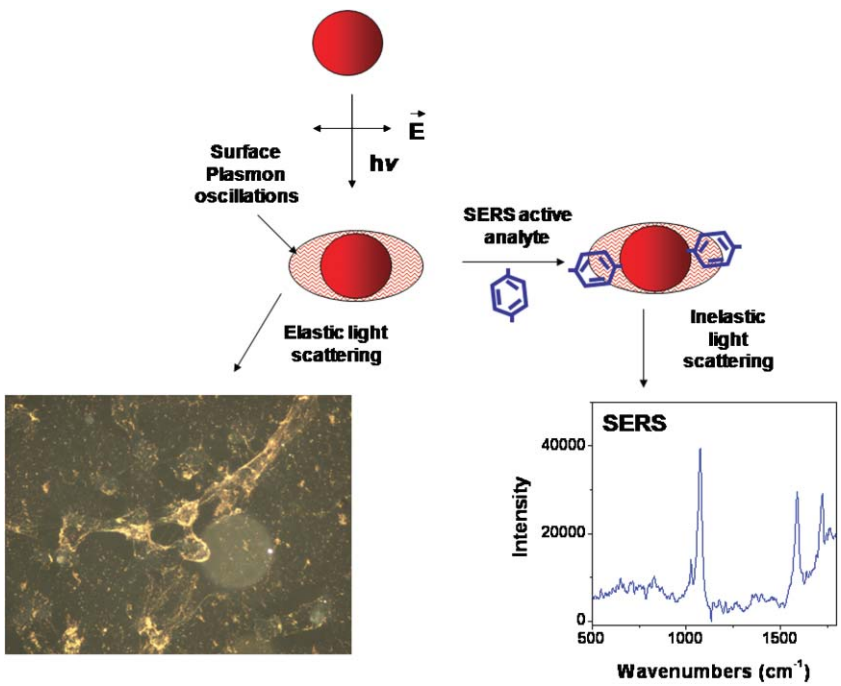

Scheme 2 Chemical sensing and imaging using scattering of light (elastic and inelastic scattering). Upon incident electromagnetic radiation that excites the surface plasmons, molecules near the nanoparticle surface undergo surface-enhanced Raman (inelastic) scattering to produce a Raman vibrational spectrum, which can be used to detect and identify near-surface molecules. Noble metal nanoparticles dispersed on a glass slide can be imaged in a darkfield optical microscope by elastically scattered visible light. The image shown here is of gold nanorods in a collagen film with cardiac cells; see the main text for further details.

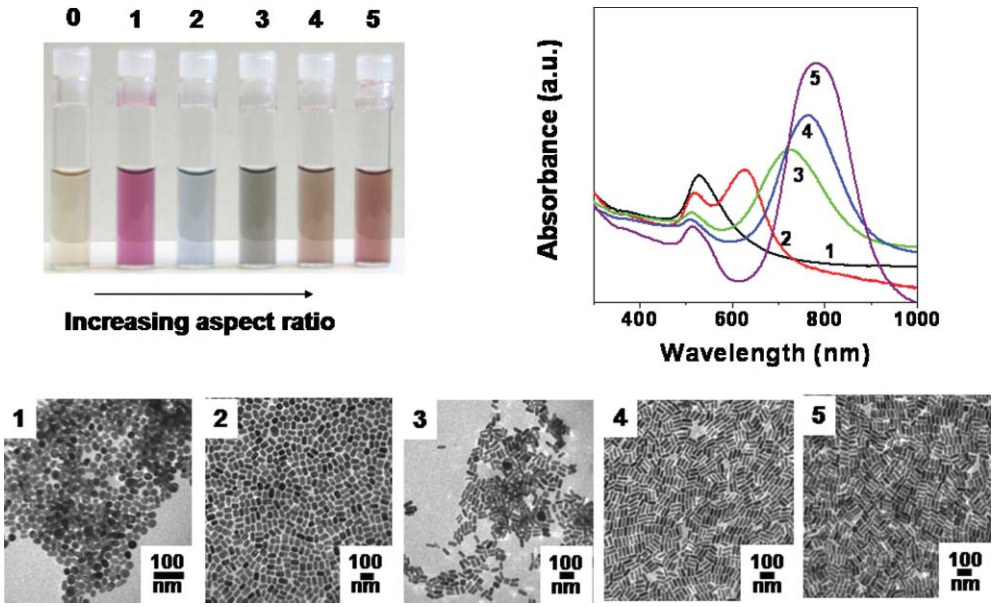

Fig. 2 The optical properties of gold and silver nanoparticles change drastically with nanoparticle shape. The photograph shows aqueous solutions of 4 nm gold nanospheres (vial 0) and progressively higher aspect ratio gold nanorods (1–5). The optical spectra and transmission electron micrographs for the particles in vials 1–5 are also shown. Scale bars in micrographs are all 100 nm.

aspect ratio.[9,29–31] For both gold and silver, the longitudinal plasmon bands that have been observed range from maxima at 500 nm to 1600 nm[29–31] (Fig. 2). Excellent reviews are available that consider theoretical descriptions of plasmons in non-spherical noble metal nanostructures.[13,21,32,33] For chemical sensing and imaging, there are some distinct advantages to noble metal nanorods compared to nanospheres. First of all, nanorods can be made that will match the frequency of common lasers (*e.g.*, 633 nm, 785 nm, or 1064 nm). Second, especially for biological applications, the use of near-infrared (NIR) light is superior to visible light because NIR light is less likely to excite background fluorescence. Third, again for biological applications, NIR light has a much greater penetration depth in tissue than visible light. Fourth, the anisotropic shape of nanorods implies different chemical reactivity at the ends vs. the middle of the rods; therefore, longitudinal and transverse plasmon bands could be independently interrogated to yield two types of chemical detection with only one type of particle.

Our group has been actively involved in the synthesis, surface modification, and applications of gold and silver anisotropic nanostructures, especially nanorods.[29–31,35–46,63,64,67–69,72] We have already described, in recent review articles, our syntheses and proposed growth mechanisms of colloidal gold and silver nanorods of controllable aspect ratio, in water.[29–31] In our work, we have identified preferential adsorption of structure-directing molecules to different crystalline faces of the growing nanoparticles as a key concept to control final nanoparticle shape. In this Feature Article, we focus on using these materials for chemical sensing and imaging applications.

Surface chemistry of nanoparticles

We have already identified two means to shift the position of the plasmon bands in noble metal nanoparticles: (1) change the local dielectric constant, or refractive index, that surrounds the particles; and (2) aggregate the nanoparticles. If we want to take advantage of these effects to do chemical sensing, then clearly it is necessary to functionalize the surface of the nanoparticles so that the analyte of interest will specifically bind, and therefore either change the local dielectric constant, or induce the nanoparticles to aggregate. Therefore, the surface chemistry of the nanomaterials plays a crucial role in sensor design.

The literature on metal nanoparticle surface modification is vast. Both organic (surfactants, bifunctional thiols, polymers, amino acids, proteins, DNA) and inorganic materials (silica, other metals, metal oxides, *etc.*) have been coated on gold and silver nanoparticles.[47–61] For gold, covalent attachment of molecules through thiols or disulfides is by far the most popular choice, which works well if the native adsorbed ions, polymers, *etc.* that were present when the nanoparticles were made are able to be displaced by Au–S bonds.[47–50,53,54]

The surfaces of one-dimensional nanostructures such as nanorods can be more distinct compared to spheres (which are usually faceted polyhedra, if crystalline). Our studies indicate that the gold nanorods synthesized by our technique (seed-mediated surfactant-directed growth) have interesting crystallographic forms.[29–31,39] Our long gold nanorods ($\sim$500 nm long, 20 nm wide) are penta-tetrahedral twinned, and display five (111) crystal faces on the ends, as opposed to (100) or (110) crystal faces on the nanorod sides.[29–31,39] This difference in crystal symmetry, we believe, is due to slightly different binding energies of our structure-directing agents to the different crystal faces of the growing nanorods.[29–31,39] In our case, it appears that the cationic surfactant used in the synthesis procedure remains on the sides of the nanorods in the form of a bilayer[62,63] which imparts an overall cationic charge to the nanomaterial, leaving the nanorod ends more available for subsequent reaction. The growth mechanism of short gold nanorods can be different, as pointed out by Guyot-Sionnest

and co-workers.[34] The introduction of Ag(I) slows down the growth, wherein the incoming gold atoms find time to be deposited at faces which are most energetically favorable.[34] Furthermore, even under acidic conditions, where Ag(I) would not be reduced by ascorbic acid to Ag(0), a monolayer of metallic silver deposits on the high energy Au{110} facets of the growing nanorod surface.[34] This is known as under-potential deposition. The Ag-monolayer-protected surface grows more slowly compared to relatively unprotected Au{100} leading to growth along the [100] direction.[34]

Surface modification of nanorods is necessary to ultimately use them for different applications. We have used bifunctional thiols such as biotin-disulfides to anchor onto the gold nanorod surface. We found that thiols bound to the Au (111) crystal face on the nanorod ends, while maintaining the CTAB bilayer protecting the nanorod sides.[64] Addition of streptavidin further leads to an end-to-end linkage of gold nanorods.[64] On similar lines, Kamat and co-workers have attached small molecules such as mercaptopropionic acid preferentially to gold nanorod ends, which in organic solvents hydrogen-bond to yield end-to-end linked nanrods.[65] In their case, too, charged surfactants that were used to grow the nanorods in solution were still present on the nanorod sides, blocking reaction there. Chang *et al.* have bound anti-mouse IgG specifically to gold nanorod ends. Subsequent addition of protein mouse IgG achieved oriented assembly of nanorods in solution.[66]

More usual, however, is to chemically modify the entire nanorod surface. We have exploited the usefulness of polyelectrolytes, which can coat the entire nanorod surface, simply based on electrostatic interactions.[67–69] Because the cationic surfactant we use in our nanorod preparations is a tetraalkylammonium salt, the nanorods are always highly positively charged independent of pH—which we can confirm with zeta potential (effective surface charge) measurements.[67–69] Following layer-by-layer electrostatic assembly techniques pioneered by others for 3-D surfaces,[51,52] we have deposited single and multiple layers of polyelectrolytes on gold nanorods by the layer-by-layer technique.[67,68] The final charged polymer coat can then be used for subsequent chemistry. For example, if we terminate the nanorod coating with a carboxylic acid-containing polymer, we can use carbodiimide coupling of acids with amines to attach amine-containing molecules to the gold nanorods through amide bonds.[68] In one example, we were able to functionalize the entire nanorod surface with biotin again, but this time using an amine-functionalized biotin.[68] Further addition of streptavidin leads to aggregation of gold nanorods in all three dimensions, not just one as we saw before with gold–thiol chemistry.[64] Using polymer coatings as a buffer layer, we have recently covalently attached antibodies and enzymes to the gold nanorods through amide bond formation and "click" chemistry.[69] Another interesting alternative to modify gold nanorods with dithiocarbamates.[70] Wei and co-workers incubated a PEG–primary amine composite with CS_2 in the presence of nanorods to give *in situ* formation of dithiocarbamate and attachment to gold nanorods.[70] This displaced CTAB in their case and controlled the non-specific cellular uptake of nanorods.[70] Another method to modify the gold nanorod surface involves replacing CTAB with phospholipids such as phosphotidylcholine (PC) using a multi-step extraction process.[71] Takahashi *et al.* demonstrated this procedure and find that PC stabilized gold nanorods have reduced cytotoxicity.[71]

We and others have shown that gold nanorods can be functionalized by silanes, and subsequent reaction can form silica coatings on gold nanorods.[72–74] Recently we have demonstrated the coating of gold nanorods with a magnetic iron oxide shell. Gold nanorods were synthesized with our usual protocol[29–31] and further coated with a single layer of the polymer polystyrene sulfonate. The resulting nanorods, now net negatively charged at neutral pH, were further reacted with a solution containing Fe(II) and Fe(III) ions (molar ratio: 0.5) and then hydroxide ions. The target product is Fe_2O_3-coated gold nanorods, which would exhibit the plasmon bands of the gold nanorods, but also would be amenable to magnetic manipulation. A further detailed investigation is being carried out in the laboratory at the present time.

Chemical sensing based on nanoparticle aggregation

Analyte-mediated gold nanoparticle aggregation has been studied to a large extent, and has been particularly useful in the detection of DNA, proteins, antibodies, glucose, toxic metal ions and other substances.[57,58,75–89] Scheme 3 shows the general idea for aggregation-based chemical sensing. Sensing is based on the coupling of plasmon resonances from particles that are within ~1 diameter of each other, upon analyte-mediated aggregation.

Mirkin and co-workers have studied in great detail the detection of DNA using gold nanoparticles.[57,58,75] They use the principle of nanoparticle aggregation due to addition of complimentary target oligonucleotide to different oligonucleotide modified gold nanoparticles.[57,58,75] On similar lines, there are reports for DNA detection using 2-D aggregation[76,77] and use of peptide nucleic acid (PNA) stabilized gold.[78] On the other hand, a new class of "molecular rulers" have been developed by Alivisatos and co-workers which rely on the red shifts in light scattering color upon DNA-directed aggregation of different surface-modified gold nanoparticles.[23,79] Aggregation based chemical sensing has also been used to detect proteins and antibodies such as anti-protein A,[80] biotin and streptavidin,[81,82] and lectins.[83,84] Different molecules such as adenosine,[85] glucose[86] have also been detected using this procedure. Detection of heavy and toxic ions such as lead,[87,88]

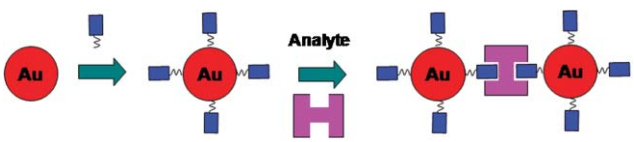

Scheme 3 A generalized scheme for chemical sensing based on gold (or silver) nanoparticles aggregation. The surface of the gold nanoparticles needs to be modified with a molecule (blue) that recognizes the analyte of interest (pink). For maximum aggregation, the analyte should bind to its partner in a multivalent fashion, so that multiple gold nanoparticles will be brought close to each other upon introduction of the analyte. The plasmon band(s) of aggregated gold and silver nanoparticles will be broadened and red-shifted as a function of aggregation state, and therefore as a function of analyte concentration.

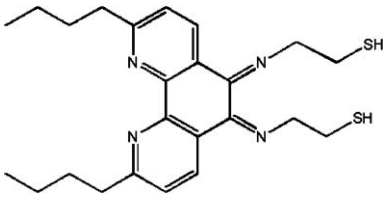

Fig. 3 Chemical structure of the modified 1,10-phenanthroline ligand that binds to gold nanoparticles through the thiols, and to lithium ion through the chelating phenanthroline nitrogens. Two ligands are required to bind to one lithium ion in a tetrahedral fashion.[89]

mercury and cadmium[88] has also been possible by studying nanoparticle aggregation. Our group has developed a lithium-ion sensor, suitable for aqueous solutions, based on gold nanoparticle aggregation that is specific for lithium ion.[89] A modified 1,10-phenanthroline ligand (Fig. 3) was synthesized and attached to 4 nm gold nanoparticles *via* the thiol ends. Lithium ions selectively bind in a 2 : 1 fashion to this ligand, causing an aggregation of ligand-modified nanoparticles when lithium ion is introduced. The colorimetric changes observed are linear with lithium ion concentration, and forms a basis of lithium ion sensing using nanoparticles (Fig. 4).[89]

In all these applications, the use of spherical nanoparticles works well. Nanorods have the advantage that the transverse and longitudinal plasmon bands are both sensitive to aggregation by broadening and red-shifting, but in two separate wavelength regimes. Therefore, depending on the constraints of the environment (*e.g.*, the presence of other chromophores, physical confinement of reaction space, *etc.*), the shape of the nanoparticle can be varied to yield optimal sensing results. The use of nanorods for sensing is relatively new and only a few reports have come out so far. We have used biotin–avidin as a model system for aggregation and change in optical properties of nanorods.[64,68] The instant aggregation of biotinylated nanorods upon addition of streptavidin forms a basis for detecting proteins such as streptavidin.[68] Chang *et al.* used the specific affinity of mouse IgG towards anti-mouse IgG to demonstrate nanorod linking. This forms a basis for sensing antibodies due to nanorod aggregation.[66] We have used the shifts in plasmon bands to monitor the aggregation of gold nanorods triggered by protonation and deprotonation of adipic acid.[90] Sudeep *et al* were able to selectively detect micro molar concentrations of cysteine and glutathione using optical spectral changes in gold nanorods.[91] The changes in optical spectra from the end-to-end linking of nanorods were due to preferential binding of cysteine to the nanorod ends.[91] In all of these examples, however, the chemistry of molecular recognition must be supplied: the nanoparticle aggregation state is dictated by their surface chemistry, and would otherwise not be specific enough.

Chemical sensing based on plasmon shifts with local refractive index

We have alluded above to the sensitivity of the position of the plasmon bands in metal nanoparticles to the local dielectric constant/refractive index. If the chemistry of the nanoparticle can be engineered so that only the analyte of interest will bind to its surface, the binding event will induce a small yet detectable change in the frequency of the plasmon band (Fig. 1). The overall shift does depend on surface coverage. A series of papers from numerous labs have laid the groundwork for correlation of plasmon band position (either observed from colloidal solutions spectrophotometrically; or from surface-bound nanoparticles scattering light in a darkfield optical microscope) with refractive index changes.[17,92–98] For gold or silver nanorods, the trends should be similar, but little experimental work has been published. As in the case of spherical particles, the shifts in plasmon bands can be used to study successful surface modification. This shift in the LSPR is due to the increase in the refractive index of the medium, as is well known for spheres. We have used the LSPR shifts as a tool to confirm surface modification of gold nanorods by polymers and biomolecules.[67–69] Similarly, Yu *et al.*, modified the gold nanorod surface with different bifunctional thiols and used the LSPR shifts to monitor surface modification of gold nanorods.[99] LSPR shifts were also observed by Liz-Marzan and co-workers at different stages in an attempt to modify the nanorod surface by polymers and silica with subsequent transfer to non-aqueous solvents.[100] Furthermore their studies also indicated that surface modification of gold nanorods leads to a shift in the longitudinal plasmon band that is much larger than that for the transverse plasmon band.[101] One report has

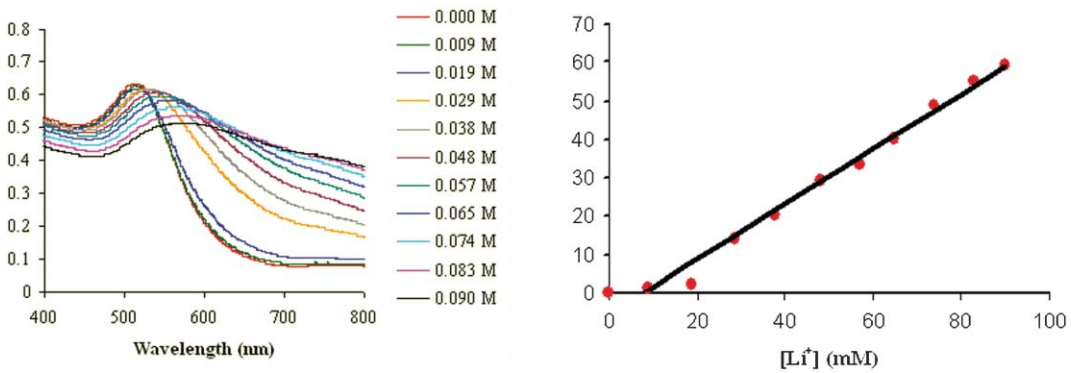

Fig. 4 Aqueous solutions of 4 nm diameter gold nanospheres, modified with the ligand of Fig. 3, change color upon lithium ion addition, due to nanoparticle aggregation. Left panel: optical spectra of solutions with various lithium ion concentrations. Right panel: calibration curve, based on plasmon band maximum shifts, from optical spectra. See ref. 89 for more details.

found that the square of the shift in peak longitudinal plasmon wavelength for gold nanorods is linear with the square of the refractive index of the medium.[102] As the longitudinal plasmon band is comparatively more sensitive than the transverse band, it can be used for sensing applications simply based on local refractive index changes. Such refractive index changes could be due to adsorption of analyte, rather than the commonly used aggregation-mediated colorimetric variation. Irudayaraj and co-workers recently demonstrate this by multiplexed detection of anti-IgG using IgG modified nanorod molecular probes (GNrMPs).[103] The red-shift in plasmon bands due to the binding of target anti-IgG to GNrMPs is solely due to refractive index changes rather than cross-linking of nanorods. This was supported by two facts. Firstly, the anti-IgG has a single binding site to which GNrMP can interact, hence ruling out head-to-tail aggregation.[103] Secondly, only the longitudinal plasmon band red-shifts significantly, as opposed to the red-shifts of both the plasmon bands, a feature generally observed for analyte mediate aggregation.[103] The same principle of using refractive index variation as a means of detection applies to thin film studies. Wang *et al*. have demonstrated the immobilization of silica-coated gold nanorods onto PVP-modified quartz substrates and their subsequent biofunctionalization by anti-human-IgG.[104] These nanorod films were further used for colorimetric detection of human IgG by calibrating the LSPR shifts in terms of IgG concentration.[104] Recently, Marinakos *et al*. performed an interesting study of using gold nanorod films for label free analyte detection using the model biotin-streptavidin binding.[105] Gold nanorods chemisorbed on glass slides modified with biotin were used to sense pM–μM concentrations of streptavidin upon binding, based on LSPR shifts. The LSPR shifts are due to the change in the local refractive index of the gold nanorods upon streptavidin binding.[105] The sensitivity of the LSPR of the nanorod film to changes in local refractive index was studied by immersing in different liquids with varying refractive indices (refractive index from 1.3 to 1.5).[105] By depositing polyelectrolyte multilayers, they were able to determine the distance dependent sensitivity of LSPR shifts of gold nanorods to refractive index changes.[105] In all these cases, the changes in the LSPR bands is due to the increase in the local refractive index of the medium surrounding the gold nanorods, as also observed for spherical nanoparticles.

For other particle shapes, van Duyne has demonstrated femtomolar detection of proteins, and zeptomolar detection of thiols (based on the LSPR shifts of individual silver nanotriangles in a darkfield optical microscope).[106] Nehl *et al*. have studied the LSPR shifts as a function of refractive index for star-shaped gold nanoparticles dispersed in water (n = 1.33), sucrose (n = 1.38) and oil (n = 1.515).[107] They determined the LSPR shifts in terms of the units eV/RIU (shift in photon energy divided by change in refractive index units). This, known as dielectric sensitivity, is a way to determine how sensitive the system is to the variation of local refractive indices, and an important parameter for using nanoparticles in biological/chemical sensing.[107] This number is different for different shapes. Taking into account the spectral line width, a figure of merit was calculated which is simply the dielectric sensitivity divided by the line width of the plasmon resonance in eV. They find that their star shaped nanoparticles showed a figure of merit that was twice than any other shape.[107] These high dielectric sensitivity particles could be ideal for sensing applications.[107] Liz-Marzan and co-workers studied the optical properties of gold decahedra as a function of local refractive index variation using experiments and theoretical modeling.[108] They found a consistent red shift in the LSPR bands upon an increase in the refractive index or an increase in the thickness of silica shell coating. Furthermore they also found a size dependence of these shifts.[108]

Chemical sensing based on inelastic light scattering: surface-enhanced Raman scattering with noble metal nanoparticles

Gold and silver nanoparticles are excellent substrates to detect molecules with surface-enhanced Raman scattering (SERS) techniques.[26,106,109–116] As mentioned in the Introduction, while the Raman effect itself is weak, the presence of nanoscale metals that efficiently interact with the incoming visible or NIR photon gives an enormous increase in the Raman signals of nearby molecules. Furthermore, the ability to tune the plasmon band of nanorods, by changing their aspect ratio, to a specific laser excitation wavelength allows one to obtain maximum enhancement. It has also been calculated that the high curvature associated with nanorods results in high surface electromagnetic fields giving particularly high enhancements known as "the lightning rod effect."[13] There are two operational mechanisms that are typically used to explain the SERS phenomenon: electromagnetic (EM) and chemical (CHEM) enhancement mechanisms. The chemical enhancement mechanism results from an electronic resonance-charge transfer between the analyte and the noble metal surface. This results in an increase in the polarizability of the analyte causing an increase in the molecule's Raman scattering. A large electromagnetic field is generated by a nanoscale surface in response to the incident light. This field interacts with the analyte situated in the vicinity of the nanoscale surface causing an enhancement in their Raman scattering.[116] Junctions between nanoparticles where these electromagnetic fields overlap will generate large field enhancements, and they may even allow for single molecule detection.[26,28] These electromagnetic fields are generated by the localized surface plasmon resonance of the nanoparticles, which can be tuned by changing the size, shape, and aggregation state of the nanoparticles.[13]

Since the introduction of SERS on roughened silver electrodes in 1977[117,118] there has been a great deal of research centered on maximizing the Raman signals from molecules adsorbed to spherical colloidal substrates of gold and silver; but until recently systematic studies of SERS as a function of particle shape have been limited. Recent developments in the controlled synthesis of gold and silver nanomaterials with well-defined, reproducible nonspherical shapes has led to something of a renaissance in SERS research.[29–31]

The use of gold and silver nanomaterials of different morphologies as SERS substrates has been reported by us and by other laboratories. Moskovits *et al*. have studied SERS on both aligned silver nanowire rafts[119] and metal–silica hybrid nanostructures.[120] In the latter work, a SERS-active

substrate consisting of silver nanoparticles on the tips of silica rods was fabricated. It was found that sub-attomolar quantities of 4-aminobenzenethiol were detectable by SERS, and that enhancement factors (in which one compares the normal Raman signal intensities of the analyte molecule to the surface-enhanced Raman signal intensities) were 10–20 times greater for bundles of silver nanoparticles at the tips of silica rods than were obtainable for analogous arrays of the silver nanorods.[120] This result is more likely due to the high number of junctions formed between silver nanoparticles on the silica posts, compared to silver nanorod arrays spaced further apart. El-Sayed and co-workers have investigated the use of both unaggregated[121] and aggregated[122] gold nanorods as SERS substrates for the detection of both pyridine and 4-aminothiophenol (4-ATP). Nikoobakht *et al.* used a 1064 nm excitation wavelength in both aggregated and unaggregated studies in order to minimize the contribution of the EM enhancement and focus on the CHEM enhancement due to the adsorption of the pyridine or 4-ATP to the gold surface. Even with little contribution from the EM enhancement mechanism for unaggregated samples they reported significant enhancements of $\sim 10^4$ for pyridine and $\sim 10^5$ for 4-ATP.[121] Aggregation of the nanorods, which produced junctions, led to an increase in the Raman signal intensities which could not be reached with an unaggregated sample. More recently the El-Sayed group has shown that human oral cancer cells can align gold nanorods that have been modified with anti-epidermal growth factor receptor antibodies on the cells surface. The alignment of the nanorods on the cells surface leads to homogeneous electromagnetic fields that were used to obtain a SERS fingerprint unique to the cancer cells.[123] Jackson and Halas have shown that large enhancement factors of 10^9–10^{10} can be observed for 4-mercaptoaniline using gold nanoshells, which are thin partial gold coats on silica nanospheres.[124] Many complex silver substrates, fixed to surfaces, have been prepared by the van Duyne group for the quantitative detection of analytes such as glucose and biowarfare agents by SERS.[116]

Theory suggests that anisotropic shapes of noble metal nanoparticles will provide the most EM enhancement for SERS—corners and edges are hot spots.[125,126] In our own work, we have attempted to answer the question "Which shape is best for SERS?" using two sets of experiments. In one set of experiments, we simply mixed various analytes in solution with colloidal gold and silver nanorods of various aspect ratios. This method is simple, but the lack of knowledge of how many junctions are formed reproducibly between particles (if any) lessens its appeal. More reproducible are fixed substrates, such as those favored by van Duyne.[127–130] In our second set of experiments, we fix the analyte to a flat gold surface, and sprinkle gold nanoparticles of various shapes on top of the analyte. This geometry is as junction-free as possible with respect to nanoparticle–nanoparticle interactions, when nanoparticle surface coverage is low; but the flat gold base does support surface plasmons as well when irradiated, which couple to the nanoparticles to provide surprisingly good Raman enhancements.

In our first set of experiments, we produced gold and silver nanorods of various aspect ratios in our usual way, covered with a bilayer of the cationic surfactant cetyltrimethylammonium bromide (CTAB).[29–31] In this case dilute colloidal solutions of the nanorods were used to minimize the effect of plasmon coupling due to nanoparticle junctions. It can be seen in the extinction spectra in Fig. 5 that silver nanorods with aspect ratio 10 and gold nanorods with aspect ratio 1.7 have the largest degree of overlap with the excitation source of 632.8 nm (He–Ne laser). Table 1 shows that the rods with the most overlap with the excitation source give 10–10^2 greater SERS enhancements than the gold and silver rods of other aspect ratios, as expected.[131] However, while trends for one molecule and several substrates can be perceived, there is little correlation, for a given substrate, as to how much the Raman signals of different molecules will be enhanced. For example, aspect ratio 3.5 silver nanorods do enhance the Raman signals from the four molecules listed, but the enhancements vary by two orders of magnitude.

Enhancement factors (EF) are typically used to calculate how large the Raman signal enhancement is for a particular vibrational mode of an analyte molecule when it is in the presence of a metallic substrate, compared to its normal Raman intensity:

$$\mathrm{EF} = \frac{(\text{SERS intensity})/\#\text{ of molecules}}{(\text{Raman intensity})/\#\text{ of molecules}} \quad (1)$$

The Raman signal intensities in Eq. 1 must be normalized to the integration time used in the measurements. The difficulty

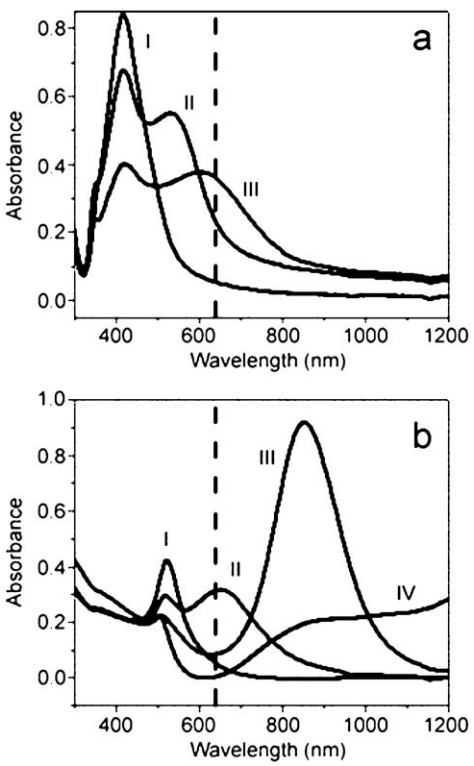

Fig. 5 Absorption spectra of (a) silver nanorods with aspect ratios 1 (trace I), 3.5 (trace II) and 10 (trace III) and (b) gold nanorods with aspect ratios 1 (trace I), 1.7 (trace II), 4.5 (trace III) and 16 (trace IV). The vertical dashed line represents the excitation wavelength for SERS measurements at 632.8 nm. Reproduced from ref. 131 with permission. Copyright 2006, PCCP Owner Societies.

Table 1 Surface enhancement factors (EF) for analytes (10^{-6} M in aqueous solution) with colloidal silver and gold nanorod and nanosphere substrates[131]

Substrate	EF for analyte/vibrational mode		
	4-Mercaptopyridine/C–C stretch	4-Aminothiophenol/C–S stretch	2,2′-Bipyridine/C–H bend
Silver nanorods, aspect ratio 10	2.3×10^7	2.3×10^6	8.5×10^5
Silver nanorods, aspect ratio 3.5	2.5×10^6	2.7×10^5	2.1×10^4
Silver nanospheres	4.8×10^6	3.9×10^5	2.6×10^4
Gold nanorods, aspect ratio 1.7	1.4×10^5	2.3×10^4	[a]
Gold nanorods, aspect ratio 4.5	6.2×10^4	4.3×10^3	[a]
Gold nanorods, aspect ratio 16	1.8×10^4	[a]	[a]
Gold nanospheres	1.2×10^4	2.0×10^3	[a]

[a] Not observed.

lies in reliable numbers for molecules sampled. In the case of simple Raman measurements in solution, the usual assumption is that the spot size of the laser defines a cylinder in the cuvette, and from this known volume and known bulk concentration, the number of molecules responsible for the normal Raman signal is readily calculated. However, in the presence of colloidal metal nanoparticles, the usual assumption for SERS is that there is a monolayer of the molecule of interest on the nanoparticles. This may not at all be true. Additional estimates of the nanoparticle concentration in solution are required to calculate the number of molecules sampled in the colloidal SERS experiment. Junction formation between nanoparticles is extremely difficult to quantitate, and this contributes a major uncertainty in enhancement factor calculations.

In our second set of experiments, gold nanorods and other particle morphologies were used to enhance the SERS signals from a self-assembled monolayer (SAM) of 4-mercaptobenzoic acid (4-MBA; a model analyte) on a smooth gold substrate (Scheme 4).[132] This geometry greatly reduces the uncertainties in estimating the number of molecules sampled, because the self-assembled monolayer coverage can be measured with reasonable accuracy to give the number of molecules per square area. Likewise, scanning electron micrographs of the immobilized nanoparticles (Fig. 6) can be used to calculate the number of nanoparticles per square area. Together, these numbers can be combined to provide a very good estimate of the number of molecules underneath the nanoparticles in the illuminated area in the SERS measurement.

Gold cubes, blocks, spheres, nanorods, dogbones and tetrapods were electrostatically immobilized on 4-MBA SAMs, creating a sandwich architecture (Scheme 4). Because 4-MBA is deprotonated under neutral or basic water conditions, and the nanoparticles are all positively charged independent of pH due to the presence of the cationic CTAB surfactant, the nanoparticles were immobilized quite well on the SAM surface, withstanding several vigorous rinsings with water. Fig. 6 shows a sample scanning electron micrograph of one of the chips used in the SERS experiments; assuming full coverage of the 4-MBA on the flat surface, one can count the number of nanoparticles per unit area to obtain a very good estimate of how many analyte molecules are being sampled in the spot size of the SERS laser. Table 2 shows the nanoparticle shapes and position of plasmon bands as observed by UV-visible spectroscopy. Our laser line for the SERS experiments was 633 nm; therefore, one would expect that nanoparticles whose plasmon bands overlap with this wavelength the most would provide the greatest SERS enhancements. However, the

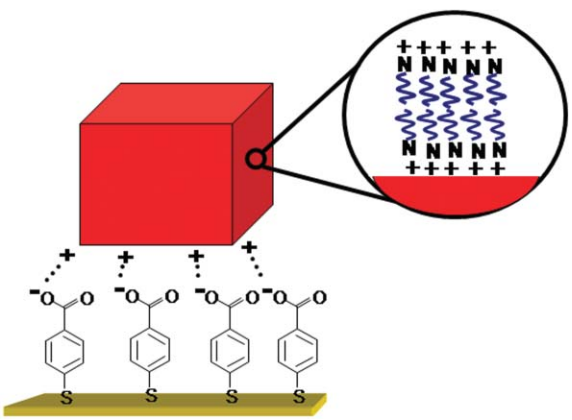

Scheme 4 Schematic showing the nanoparticle-SAM sandwich geometry.[132] A self-assembled monolayer of 4-mercaptobenzoic acid on a flat gold surface is washed in basic aqueous solution to deprotonate the carboxylic acids. Gold nanocubes, far larger than single molecules, adsorb electrostatically to the surface due to the net positive charge of the cationic surfactant, cetyltrimethylammonium bromide, that is bound to the nanocube surface as a bilayer. The CTAB bilayer that is adsorbed to the nanoparticle surface is depicted in the inset.

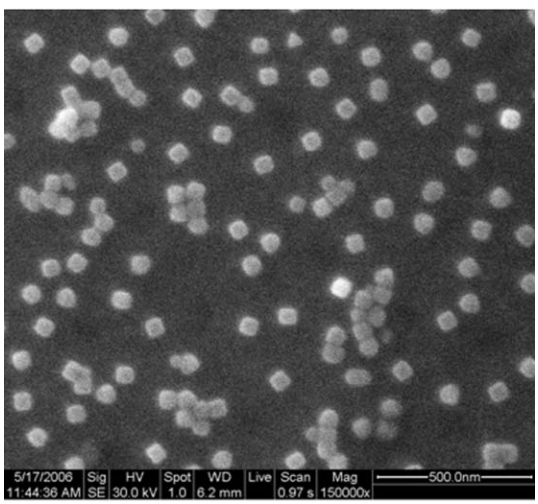

Fig. 6 Scanning electron micrograph of gold nanocubes electrostatically immobilized on a self-assembled monolayer of 4-mercaptobenzoic acid on flat gold. Scale bar = 500 nm.

Table 2 Gold nanoparticle shape dependence of SERS enhancement factors in SAM sandwich geometry experiments.[132] The enhancement factors were similar for all aspect ratio of nanorods tested (3–16) for the 633 nm excitation used

Nanoparticle shape	Nanoparticle dimensions/nm	Plasmon band maxima/nm	SERS enhancement factor
Spheres	Diameter = 29 ± 6	520	(1.62 ± 0.63) × 10^7
Nanorods, aspect ratio 16	Width = 23 ± 4 Length = 372 ± 119	515, >1200	(1.08 ± 0.08) × 10^8
Tetrapods	Center width = 81 ± 18 Edge length = 107 ± 18	515, 670	(7.16 ± 0.09) × 10^8
Dogbones	Center width = 21 ± 2 End width = 30 ± 4 Length = 68 ± 11	515, 580, 800	(1.61 ± 0.11) × 10^9
Cubes	Edge length = 61 ± 3	520, 950	(2.47 ± 0.21) × 10^9

resulting enhancement factors in Table 2 show this is not the case; the largest enhancement comes from cubes, blocks, and dogbones. This suggests that the enhancements seen in SERS, although originating from the hotspot formed by the plasmon coupling between the LSPR on the nanoparticles and the surface plasmon of the flat gold substrate, are influenced by other factors. These other influences could include surface structure and sharpness of the structural features of the nanoparticles; and indeed, cubes and blocks have four corners down facing the analyte, while nanorods have only two ends that are close to the analyte if lying down on their sides.[132]

As has been pointed out by others[133] a more practical measure of how useful SERS is as a detection technique is to estimate the limit of detection for analytes, rather than what enhancement factors they produce with a given SERS substrate. This is becoming more common in the literature; for example, van Duyne estimates a limit of detection of ~1400 anthrax spores, based on SERS – if the 1400 spores are captured by the substrate.[134]

Optical imaging with gold nanorods

Spatial visualization of gold and silver nanoparticles has been performed by a number of groups using darkfield optical microscopy.[135–137] The signal from the metallic nanoparticles is based on elastic light scattering in this technique; therefore, if one wanted to monitor the position of nanoparticles noninvasively, darkfield microscopy is a good choice if the matrix is not too scattering itself. The spot size of the scattered light can be far larger than the actual size of the nanoparticles, and spatial resolution is typically limited by optics to ~200 nm.

The use of metallic nanoparticles to image some sort of chemical, physical, or biological process is growing. Early examples include using silver nanoparticles of various sizes to infer effective transport pore size in bacterial membranes, in living cells.[138] Nanorods, and other anisotropic shapes, absorb strongly in the near-infrared (NIR) portion of the electromagnetic spectrum. The absorbed radiation can be emitted as heat or emission (fluorescence). There have been reports on weak fluorescence emission of gold nanoparticles.[139] El-Sayed and co-workers found that gold nanorods exhibit linear fluorescence in the visible with a quantum yield of ~10^{-4} and is enhanced compared to spheres which was theoretically modeled as lightning rod effect.[140] They further find that the enhanced fluorescence depends on the aspect ratio of the nanorods.[141] Furthermore, the fluorescence properties of gold nanorods have also been used for DNA sensing.[142] Despite this, the fluorescence quantum yields of nanorods are significantly lower than organic dyes or quantum dots. Hence, most of the incident energy absorbed by the nanorods is converted to heat. Several groups have combined darkfield optical microscopy imaging of nanorod position with this engineered local photodamage capability to use gold nanorods as imagers and photothermal destroyers of cancer cells.[135,143,144] In these applications, the surface chemistry of the nanorods must be tuned so that the nanorods bind selectively to the desired cellular target. Similarly, gold nanoshells and nanocages have also been used as photothermal destroyers.[145,146]

Recently, our group has used darkfield microscopic imaging of gold nanorod position to measure materials properties such as local strain, in both polymer films and biological systems.[147,148] Classic engineering strain is defined as $\varepsilon = \Delta l/l$ where ε is strain, l is the original length of the material, and Δl is the change in length (final minus initial) in response to a load. Strain may be positive (tensile) or negative (compressive), and can be measured in all three dimensions (x, y, z). By visualizing the positions of gold nanorods in a matrix as it is deformed, digital image correlation software can be used to create maps of strain across the matrix. If the load is homogeneous, one would expect the strain fields across the material to be homogeneous (if the material itself is homogeneous). More interesting is to measure local positional displacements that track local strain fields.

In our work we used gold nanorods to track deformations in two polymer films, poly(vinyl alcohol) (PVA) and polydimethylsiloxane (PDMS) as they were manually stretched.[147] Gold nanorods (372 ± 119 nm in length and 23 ± 4 nm in width) were mixed with both polymers as fluids and allowed to cure. The films were then subsequently stretched to 25% of their initial length (for PVA) and 20% of initial length (for PDMS). Darkfield images were taken before and after stretching for both samples. With locally developed digital image correlation software, nanorod displacements were converted into strain fields; the nanorods move as the films are stretched, and the software maps spatial locations in the original undeformed state and compares this to the post-stretched films (Fig. 7). In Fig. 7, the top panel shows, in color form, the displacement of gold nanorods upon stretching to the left (blue) and right (red). The expected strain is colored green in the center panel, with lower and higher values toward blue and red respectively. Notice that the resulting strain field

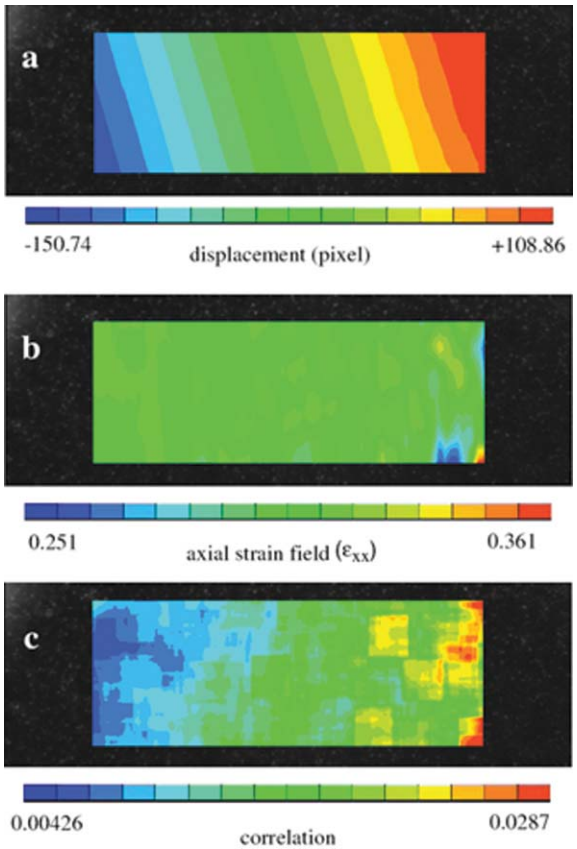

Fig. 7 Results of image correlation for uniaxial tension in the horizontal direction for PVA. (a) Axial displacement field resulting from the ends of the film being pulled in opposite directions. Blue indicates movement to the left, red indicates movement to the right. (b) The calculated axial strain field (labeled ε_{xx}) from the gold nanorod darkfield data, showing a roughly uniform field of the expected value (green). (c) The correlation error, calculated over the sample, from blue (lower) to red (higher). Reproduced from ref. 147 with permission. Copyright 2005, Institute of Physics.

map across the material (approx. 1 mm field of view) is mostly green, indicating that the expected strain matched the experimentally determined one. Furthermore, the correlation values (bottom panel of Fig. 7), which are measure of the software's accuracy, were $\sim$1% of the strain field values in the middle panel. The results for PDMS, a more hydrophobic polymer than PVA, were similar. Overall, this study suggested that gold nanorods could be used as a novel imaging agent to measure mechanical properties, a ''nano strain gauge.''

In recent work[148] we used the same technique—darkfield microscopy of gold nanorods combined with digital image correlation software—to map inhomogeneous strain fields across a biological system: cardiac cells in a collagen matrix.[148] Collagen is the main structural protein in the body, including the heart; and heart cells (myocytes are the beaters; fibroblasts are the support system) send out extensions to manipulate their local mechanical environment. It is well-known in biology that a cell responds to changes in its mechanical environment and that this response is critical to cell/tissue function. There have been many studies in this area in which physical cues, transmitted through a collagenous network, are

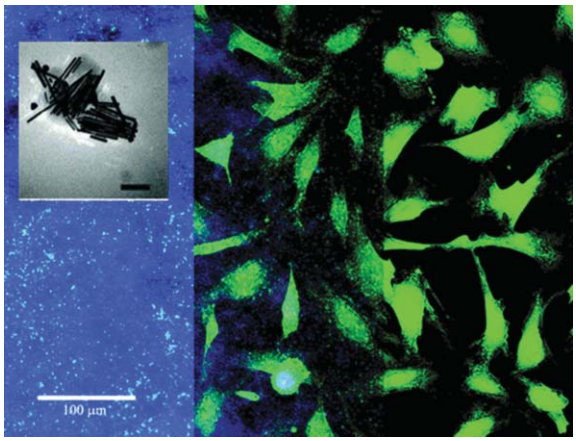

Fig. 8 Darkfield optical micrograph of light scattered from gold nanorods (left panel). Simultaneous fluorescence image of cardiac fibroblasts (right panel). The two images superimposed with some transparency (center panel). Scale bar: 100 μm. Inset: transmission electron micrograph of the gold nanorods. Inset scale bar: 100 nm. Reproduced from ref. 148 with permission. Copyright 2007, American Chemical Society.

used to trigger mechanical and biochemical responses by different types of cells.[149–156]

In our work gold nanorods (376 $\pm$ 105 nm long, 26 $\pm$ 5 nm wide) were prepared and introduced into thin collagen films. These films were then subsequently plated with neonatal rat cardiac fibroblasts that were stained with a fluorescent dye. Fig. 8 is a composite image showing scattering from gold nanorods in collagen (left panel), stained cardiac fibroblasts (right panel) and an overlay of the two (center panel).

Images were collected over a 2 h time interval from 5–7 h after cells were plated. During this time, the cells moved, sent out extensions, and generated local strain fields in doing so. Nanorod positions changed as a result of the cellular activity, and from the positional displacements of the nanorods as a function of time, strain fields could be calculated as a function of time using the same software as above. Fig. 9 is the complete set of strain fields, evolving over time, for horizontal strains generated between 320 and 420 min after cell plating. Strain fields were calculated from the darkfield pixel intensities of gold nanorods embedded in the collagen films. Notice that the fields here are distinctly not homogeneous: this is because the sample is not homogeneous. In our case, and over this relatively short time span, we observed axial tensile strains near 0.003, which compares well to what might be expected for cells in this situation.

In principle, any small enough object that emits or scatters light could be used to measure strain fields using the appropriate software. Compared to fluorescent dyes, gold nanorods have distinct advantages: they absorb in the NIR, far from tissue interferents; they do not photobleach as do organic dyes; they can monitor events on the $\sim$200 nm scale and larger, to capture information about what happens between cells; and they appear to be nontoxic.[135,148,157]

Even though gold nanorods do not have a strong linear fluorescence (quantum yield $\sim 10^{-4}$)—in fact, they typically quench fluorescence of nearby fluorophores—there have been

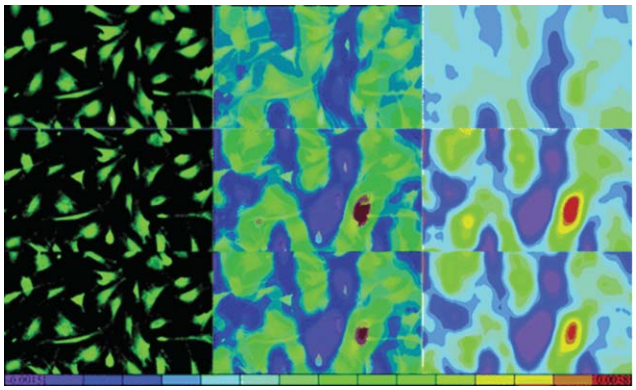

Fig. 9 Cells and corresponding strain field maps: row 1, t = 320 min; row 2, t = 400 min; row 3, t = 420 min. In each row, left to right, are images of the fluorescently tagged cells, a transparent overlay of strain fields on cells, and the calculated strain fields from gold nanorod positions. Violet indicates the maximum compressive strain and red the maximum tensile strain. Color scale at the bottom runs from violet −0.0015 (compressive) to 0.0038 (tensile) strain. Reproduced from ref. 148 with permission. Copyright 2007, American Chemical Society.

recent interesting reports of their nonlinear optical properties that are also amenable to imaging applications. For example, a recent report finds metallic nanoparticles, when excited with a femtosecond Ti:sapphire laser, are capable of exhibiting two-photon luminescence (TPL).[158] Gold nanorods were prepared having a longitudinal plasmon band centered around 820 nm and were subsequently excited at 830 nm on a far-field laser-scanning microscope in order to produce TPL.[159] The TPL was found to be 58 times greater in intensity than the TPL from a single rhodamine molecule, which is considered to be a standard bright fluorophore. Single gold nanorods were imaged both in *vitro* and in *vivo* in the blood vessels of a mouse ear using TPL.[159] It was found that the uniform intensities of the TPL in the single-frame images indicated that most of the observed were those of single nanorods. In addition, the resulting intensity of the TPL was three times greater for the gold nanorods than for the blood and tissue occupying the matrix. Related TPL experiments by others showed that gold nanorods are excellent contrast agents for cancer cells, if appropriately functionalized on their surfaces so they specifically bind to cancer cells.[160]

Another example of gold nanorods in biological imaging is based on the thermal properties of tissues. Motamedi and co-workers[161] used LOIS (laser optoacoustic imaging system) to detect and image gold nanorods deep within nude mice tissue. LOIS is an imaging technique used widely in medicine; it is based on flashing the targeted area with a low energy laser in the NIR region. The NIR radiation can penetrate deeply into biological tissue and a fraction of this light will be absorbed by the tissue. The absorbed light will expand the tissue through thermoelastic expansion. This expansion creates ultrasonic acoustic waves that can be detected. LOIS was used to visualize the distribution of gold nanorods at a concentration as low as 125 pM delivered subcutaneously to the mice. Gold nanorods in that study was superior compared to spherical gold nanoparticles since the latter absorb light only in the visible region (λ = 520 nm).

Conclusions

The advent of improved nanoparticle synthetic methods, coupled with increasingly sophisticated theory and experimental affirmation of their shape-dependent optical properties, is jump-starting really exciting work in the areas of chemical sensing and imaging. Gold nanorods in particular have many attractive properties: their plasmon bands can be tuned throughout the visible and near-infrared portions of the electromagnetic spectrum, depending on their aspect ratio (length/width ratio); they are excellent substrates for surface-enhanced Raman scattering, as well as other surface-enhanced spectroscopies; they can undergo two-photon photoluminescence; they elastically scatter light well. In the not-too-distant future, one can imagine that the sensitivity of the nanorods for their local chemical environment can be coupled with their imaging capability, and result in new tools to measure chemical, physical, and biological phenomena on the sub-micron scale in real time.

Acknowledgements

We thank the U.S. National Science Foundation, the W. M. Keck Foundation, and the University of South Carolina for their support. We also thank our many colleagues, collaborators, and former members of the Murphy group who have inspired and guided us.

References

1 S. J. Williamson and H. Z. Cummins, *Light and Color in Nature and Art*, Wiley, New York, 1983.
2 D. L. Feldheim and C. A. Foss, Jr., in *Metal Nanoparticles: Synthesis, Characterization, and Applications*, ed. D. L. Feldheim and C. A. Foss, Jr., Marcel Dekker, New York, 2002.
3 *Understanding Nanotechnology*, edited by the staff of Scientific American, Warner Books, New York, 2002.
4 A. P. Alivisatos, *Science*, 1996, **271**, 933.
5 G. Cao, *Nanostructures & Nanomaterials: Synthesis, Properties & Applications*, Imperial College Press, London, 2004.
6 C. J. Murphy and J. L. Coffer, *Appl. Spectrosc.*, 2002, **56**, 16A.
7 C.-A. J. Lin, T. Liedl, R. A. Sperling, M. T. Fernandez-Arguelles, J. M. Costa Fernandez, R. Pereiro, A. Sanz-Medel, W. H. Chang and W. J. Parak, *J. Mater. Chem.*, 2007, **17**, 1343.
8 E. H. Sargent, *Adv. Mater.*, 2005, **17**, 515.
9 M. A. El-Sayed, *Acc. Chem. Res.*, 2001, **34**, 257.
10 M.-C. Daniel and D. Astruc, *Chem. Rev.*, 2004, **104**, 293.
11 A. J. Haes, D. A. Stuart, S. Nie and R. P. Van Duyne, *J. Fluoresc.*, 2004, **14**, 355.
12 K. L. Kelly, T. R. Jensen, A. A. Lazarides and G. C. Schatz, in *Metal Nanoparticles: Synthesis, Characterization, and Applications*, ed. D. L. Feldheim and C. A. Foss, Jr., Marcel Dekker, New York, 2002.
13 K. L. Kelly, E. Coronado, L. L. Zhao and G. C. Schatz, *J. Phys. Chem. B*, 2003, **107**, 668.
14 U. Kreibig and M. Vollmer, *Optical Properties of Metal Clusters*, Springer-Verlag, Berlin, 1996.
15 A. Henglein, *Chem. Rev.*, 1989, **89**, 1861.
16 G. Mie, *Ann. Phys.*, 1908, **330**, 377.
17 A. C. Templeton, J. J. Pietron, R. W. Murray and P. Mulvaney, *J. Phys. Chem. B*, 2000, **104**, 564.
18 A. N. Shipway, M. Lahav, R. Gabai and I. Willner, *Langmuir*, 2000, **16**, 8789.
19 M. Gluodenis and C. A. Foss, Jr., *J. Phys. Chem. B*, 2002, **106**, 9484.
20 J. J. Mock, M. Barbic, D. R. Smith, D. A. Schultz and S. Schultz, *J. Chem. Phys.*, 2003, **116**, 6755.

21 I. O. Sosa, C. Noguez and R. G. Barrera, *J. Phys. Chem. B*, 2003, **107**, 6269.
22 G. Raschke, S. Kowarik, T. Franzl, C. Sonnichsen, T. A. Klar, J. Feldmann, A. Nichtl and K. Kurzinger, *Nano Lett.*, 2003, **3**, 935.
23 C. Sonnichsen, B. M. Reinhard, J. Liphardt and A. P. Alivisatos, *Nat. Biotechnol.*, 2005, **23**, 741.
24 A. J. Haes, S. Zou, G. C. Schatz and R. P. Van Duyne, *J. Phys. Chem. B*, 2004, **108**, 109.
25 E. Hutter and J. H. Fendler, *Adv. Mater.*, 2004, **16**, 1685.
26 C. L. Haynes, A. D. McFarland and R. P. Van Duyne, *Anal. Chem.*, 2005, **77**, 338A.
27 S. Nie and S. R. Emory, *Science*, 1997, **275**, 1102.
28 K. Kneipp, Y. Wang, H. Kneipp, L. T. Perelman, I. Itzkan, R. R. Dasari and M. S. Feld, *Phys. Rev. Lett.*, 1997, **78**, 1667.
29 C. J. Murphy, A. M. Gole, S. E. Hunyadi and C. J. Orendorff, *Inorg. Chem.*, 2006, **45**, 7544.
30 C. J. Murphy, T. K. Sau, A. M. Gole, C. J. Orendorff, J. Gao, L. Gou, S. E. Hunyadi and T. Li, *J. Phys. Chem. B*, 2005, **109**, 13857.
31 C. J. Murphy, T. K. Sau, A. Gole and C. J. Orendorff, *MRS Bull.*, 2005, **30**, 349.
32 M. Miller and A. A. Lazarides, *J. Phys. Chem. B*, 2005, **109**, 21556.
33 N. Halas, *MRS Bull.*, 2005, **30**, 362.
34 M. Liu and P. Guyot-Sionnest, *J. Phys. Chem. B*, 2005, **109**, 22192.
35 N. R. Jana, L. Gearheart and C. J. Murphy, *Adv. Mater.*, 2001, **13**, 1389.
36 N. R. Jana, L. Gearheart and C. J. Murphy, *J. Phys. Chem. B*, 2001, **105**, 4065.
37 N. R. Jana, L. Gearheart and C. J. Murphy, *Chem. Commun.*, 2001, 617.
38 C. J. Murphy and N. R. Jana, *Adv. Mater.*, 2002, **14**, 80.
39 C. J. Johnson, E. Dujardin, S. A. Davis, C. J. Murphy and S. Mann, *J. Mater. Chem.*, 2002, **12**, 1765.
40 B. D. Busbee, S. O. Obare and C. J. Murphy, *Adv. Mater.*, 2003, **15**, 414.
41 K. K. Caswell, C. M. Bender and C. J. Murphy, *Nano Lett.*, 2003, **3**, 667.
42 J. Gao, C. M. Bender and C. J. Murphy, *Langmuir*, 2003, **19**, 9065.
43 T. K. Sau and C. J. Murphy, *Langmuir*, 2004, **20**, 6416.
44 T. K. Sau and C. J. Murphy, *J. Am. Chem. Soc.*, 2004, **126**, 8648.
45 A. Gole and C. J. Murphy, *Chem. Mater.*, 2004, **16**, 3633.
46 L. Gou and C. J. Murphy, *Chem. Mater.*, 2005, **17**, 3668.
47 M. Brust, M. Walker, D. Bethell, D. J. Schiffrin and R. Whyman, *J. Chem. Soc., Chem. Commun.*, 1994, 801.
48 V. L. Colvin, A. N. Goldstein and A. P. Alivisatos, *J. Am. Chem. Soc.*, 1992, **114**, 5221.
49 A. C. Templeton, W. P. Wuelfing and R. W. Murray, *Acc. Chem. Res.*, 2000, **33**, 27.
50 R. Shenhar and V. M. Rotello, *Acc. Chem. Res.*, 2003, **36**, 549.
51 F. Caruso, R. A. Caruso and H. Mohwald, *Science*, 1998, **282**, 1111.
52 D. I. Gittins and F. Caruso, *J. Phys. Chem. B*, 2001, **105**, 6846.
53 S. Mandal, A. Gole, N. Lala, R. Gonnade, V. Ganvir and M. Sastry, *Langmuir*, 2001, **17**, 6262.
54 C. M. Niemeyer, *Angew. Chem., Int. Ed.*, 2001, **40**, 4128.
55 E. Dujardin and S. Mann, *Adv. Mater.*, 2002, **14**, 775.
56 M. Zayats, R. Baron, I. Popov and I. Willner, *Nano Lett.*, 2005, **5**, 21.
57 C. A. Mirkin, R. L. Letsinger, R. C. Mucic and J. J. Storhoff, *Nature*, 1996, **382**, 607.
58 J. J. Storhoff, R. Elghanian, R. C. Mucic, C. A. Mirkin and R. L. Letsinger, *J. Am. Chem. Soc.*, 1998, **120**, 1959.
59 L. M. Liz-Marza'n, M. Giersig and P. Mulvaney, *Langmuir*, 1996, **12**, 4329.
60 S. Liu and M. Han, *Adv. Funct. Mater.*, 2005, **15**, 961.
61 K. S. Mayya, D. I. Gittins and F. Caruso, *Chem. Mater.*, 2001, **13**, 3833.
62 B. Nikoobakht and M. A. El-Sayed, *Langmuir*, 2001, **17**, 6368.
63 T. K. Sau and C. J. Murphy, *Langmuir*, 2005, **21**, 2923.
64 K. K. Caswell, J. N. Wilson, U. H. F. Bunz and C. J. Murphy, *J. Am. Chem. Soc.*, 2003, **125**, 13914.
65 K. G. Thomas, S. Barazzouk, B. I. Ipe, S. T. S. Joseph and P. V. Kamat, *J. Phys. Chem. B*, 2004, **108**, 13066.
66 J.-Y. Chang, H. Wu, H. Chen, Y. C. Ling and W. Tan, *Chem. Commun.*, 2005, **8**, 1092.
67 A. Gole and C. J. Murphy, *Chem. Mater.*, 2005, **17**, 1325.
68 A. Gole and C. J. Murphy, *Langmuir*, 2005, **21**, 10756.
69 A. Gole and C. J. Murphy, *Langmuir*, submitted.
70 T. B. Huff, M. N. Hansen, Y. Zhao, J.-X. Cheng and A. Wei, *Langmuir*, 2007, **23**, 1596.
71 H. Takahashi, Y. Niidome, T. Niidome, K. Kaneko, H. Kawasaki and S. Yamada, *Langmuir*, 2006, **22**, 2.
72 S. O. Obare, N. R. Jana and C. J. Murphy, *Nano Lett.*, 2001, **1**, 601.
73 S. S. Chang, C. W. Shih, C. D. Chen, W. C. Lai and C. R. C. Wang, *Langmuir*, 1999, **15**, 701.
74 V. I. Boev, J. Perez-Juste, I. Pastoriza-Santos, C. J. R. Silva, M. de Gomes and L. M. Liz-Marzan, *Langmuir*, 2004, **20**, 10268.
75 N. L. Rosi and C. A. Mirkin, *Chem. Rev.*, 2005, **105**, 1547.
76 A. Charrier, N. Candoni and F. Thibaudau, *J. Phys. Chem. B*, 2006, **110**, 12896.
77 A. Charrier, N. Candoni, N. Liachenko and F. Thibaudau, *Biosens. Bioelectron.*, 2007, **22**, 1881.
78 R. Chakrabarti and A. M. Klibanov, *J. Am. Chem. Soc.*, 2003, **125**, 12531.
79 B. M. Reinhard, M. Siu, H. Agarwal, A. P. Alivisatos and J. Liphardt, *Nano Lett.*, 2005, **5**, 2246.
80 N. T. K. Thanh and Z. Rosenzweig, *Anal. Chem.*, 2002, **74**, 1624.
81 M. Sastry, N. Lala, V. Patil, S. B. Chavan and A. G. Chittiboyina, *Langmuir*, 1998, **14**, 4138.
82 S. Fullam, S. N. Rao and D. Fitzmaurice, *J. Phys. Chem. B*, 2000, **104**, 6164.
83 H. Otsuka, Y. Akiyama, Y. Nagasaki and K. Kataoka, *J. Am. Chem. Soc.*, 2001, **123**, 8226.
84 S. Lee and V. H. Perez-Luna, *Anal. Chem.*, 2005, **77**, 7204.
85 J. Liu and Y. Lu, *Org. Biomol. Chem.*, 2006, **4**, 3435.
86 K. Aslan, J. Zhang, J. R. Lakowicz and C. D. Geddes, *J. Fluoresc.*, 2004, **14**, 391.
87 J. Liu and Y. Lu, *Anal. Chem.*, 2004, **76**, 1627.
88 Y. Kim, R. C. Johnson and J. T. Hupp, *Nano Lett.*, 2001, **1**, 165.
89 S. O. Obare, R. E. Hollowell and C. J. Murphy, *Langmuir*, 2002, **18**, 10407.
90 C. J. Orendorff, P. L. Hankins and C. J. Murphy, *Langmuir*, 2005, **21**, 2022.
91 P. K. Sudeep, S. T. S. Joseph and K. G. Thomas, *J. Am. Chem. Soc.*, 2005, **127**, 6516.
92 S. Underwood and P. Mulvaney, *Langmuir*, 1994, **10**, 3427.
93 J. J. Mock, D. R. Smith and S. Schultz, *Nano Lett.*, 2003, **3**, 485.
94 Y. G. Sun and Y. N. Xia, *Anal. Chem.*, 2002, **74**, 5297.
95 N. K. Grady, N. J. Halas and P. Nordlander, *Chem. Phys. Lett.*, 2004, **399**, 167.
96 J. J. Mock, D. R. Smith and S. Schultz, *Nano Lett.*, 2003, **3**, 485.
97 A. Curry, G. Nusz, A. Chilkoti and A. Wax, *Opt. Express*, 2005, **7**, 2668.
98 F. Tam, C. Moran and N. Halas, *J. Phys. Chem. B*, 2004, **108**, 17290.
99 C. Yu, L. Varghese and J. Irudayaraj, *Langmuir*, 2007, **23**, 9114.
100 I. Pastoriza-Santos, J. Perez-Juste and L. M. Liz-Marzan, *Chem. Mater.*, 2006, **18**, 2465.
101 J. Perez-Juste, I. Pastoriza-Santos, L. M. Liz-Marzan and P. Mulvaney, *Coord. Chem. Rev.*, 2005, **249**, 1870.
102 J. Yang, J.-C. Wu, Y.-C. Wu, J.-K. Wang and C.-C. Chen, *Chem. Phys. Lett.*, 2005, **416**, 215.
103 C. Yu and J. Irudayaraj, *Anal. Chem.*, 2007, **79**, 572.
104 C. Wang, Z. Ma, T. Wang and Z. Su, *Adv. Funct. Mater.*, 2006, **16**, 1673.
105 S. M. Marinakos, S. Chen and A. Chilkoti, *Anal. Chem.*, 2007, **79**, 5278.
106 A. J. Haes and R. P. van Duyne, *J. Am. Chem. Soc.*, 2002, **124**, 10596.
107 C. L. Nehl, H. Liao and J. H. Hafner, *Nano Lett.*, 2006, **6**, 683.
108 I. Pastoriza-Santos, A. Sanchez-Iglesias, F. J. Garcia de Abajo and L. M. Liz-Marzan, *Adv. Funct. Mater.*, 2007, **17**, 1443.
109 A. Campion and P. Kambhampati, *Chem. Soc. Rev.*, 1998, **27**, 241.

110 K. Kneipp, H. Kneipp, I. Itzkan, R. R. Dasari and M. S. Feld, *Chem. Rev.*, 1999, **99**, 2957.
111 J. A. Dieringer, A. D. McFarland, N. C. Shah, D. A. Stuart, A. V. Whitney, C. R. Yonzon, M. A. Young, X. Zhang and R. P. van Duyne, *Faraday Discuss.*, 2006, **132**, 9.
112 M. J. Natan, *Faraday Discuss.*, 2006, **132**, 321.
113 M. Moskovits, *J. Raman Spectrosc.*, 2005, **36**, 485.
114 R. F. Aroca, R. A. Alvarez-Puebla, N. Pieczonka, S. Sanchez-Cortez and J. V. Garcia-Ramos, *Adv. Colloid Interface Sci.*, 2005, **116**, 45.
115 G. C. Schatz, *Acc. Chem. Res.*, 1984, **17**, 370.
116 C. L. Haynes, C. R. Yonzon, X. Zhang and R. P. Van Duyne, *J. Raman Spectrosc.*, 2005, **36**, 471.
117 D. L. Jeanmaire and R. P. Van Duyne, *J. Electroanal. Chem.*, 1977, **84**, 1.
118 M. G. Albrecht and J. A. Creighton, *J. Am. Chem. Soc.*, 1977, **99**, 5215.
119 D. H. Jeong, Y. X. Zhang and M. Moskovits, *J. Phys. Chem. B*, 2004, **108**, 12724.
120 M. Schierhorn, S. J. Lee, S. W. Boettcher, G. D. Stucky and M. Moskovits, *Adv. Mater.*, 2006, **18**, 2829.
121 B. Nikoobakht, J. Wang and M. A. El-Sayed, *Chem. Phys. Lett.*, 2002, **366**, 17.
122 B. Nikoobakht and M. A. El-Sayed, *J. Phys. Chem. A*, 2003, **107**, 3372.
123 X. Huang, I. El-Sayed, W. Qian and M. A. El-Sayed, *Nano Lett.*, 2007, **7**, 1591.
124 J. B. Jackson and N. J. Halas, *Proc. Natl. Acad. Sci. U. S. A.*, 2004, **52**, 17930.
125 X. Hu, J. Aizpurua, M. Kall and P. Apell, *Phys. Rev. E*, 2000, **62**, 4318.
126 J. Jiang, K. Bosnich, M. Maillard and L. Brus, *J. Phys. Chem. B*, 2003, **107**, 9964.
127 C. L. Haynes, A. J. Haes and R. P. Van Duyne, *Mater. Res. Soc. Symp. Proc.*, 2001, 635.
128 X. Zhang, C. R. Yonzon and R. P. Van Duyne, *J. Mater. Res.*, 2006, **21**, 1083.
129 E. M. Hicks, O. Lyandres, W. P. Hall, S. Zou, M. R. Glucksberg and R. P. Van Duyne, *J. Phys. Chem. C*, 2007, **111**, 4116.
130 J. A. Dieringer, A. D. McFarland, N. C. Shah, D. A. Stuart, A. V. Whitney, C. R. Yonzon, M. A. Young, X. Zhang and R. P. Van Duyne, *Faraday Discuss.*, 2006, **132**, 9.
131 C. J. Orendorff, L. Gearheart, N. R. Jana and C. J. Murphy, *Phys. Chem. Chem. Phys.*, 2006, **6**, 165.
132 C. J. Orendorff, A. Gole, T. K. Sau and C. J. Murphy, *Anal. Chem.*, 2005, **77**, 3261.
133 M. J. Natan, *Faraday Discuss.*, 2006, **132**, 321.
134 X. Zhang, J. Zhao, A. V. Whitney, J. W. Elam and R. P. van Duyne, *J. Am. Chem. Soc.*, 2006, **128**, 10304.
135 X. Huang, E. H. El-Sayed, W. Zian and M. A. El-Sayed, *J. Am. Chem. Soc.*, 2006, **128**, 2115.
136 J. J. Mock, D. R. Smith and S. Schultz, *Nano Lett.*, 2003, **3**, 485.
137 J. J. Mock, M. Barbic, D. R. Smith, D. A. Schultz and S. Schultz, *J. Chem. Phys.*, 2002, **116**, 6755.
138 X. N. Xu, J. Chen, R. B. Jeffers and S. Kyriacou, *Nano Lett.*, 2002, **2**, 175.
139 G. Wang, T. Huang, R. W. Murray, L. Menard and R. G. Nuzzo, *J. Am. Chem. Soc.*, 2005, **127**, 812.
140 M. B. Mohamed, V. Volkov, S. Link and M. A. El-Sayed, *Chem. Phys. Lett.*, 2000, **317**, 517.
141 S. Eustis and M. El-Sayed, *J. Phys. Chem. B*, 2005, **109**, 16350.
142 C.-Z. Li, K. B. Male, S. Hrapovic and J. H. T. Luong, *Chem. Commun.*, 2005, 3924.
143 H. Takahashi, T. Niidome, A. Nariai, Y. Niidome and S. Yamada, *Chem. Lett.*, 2006, **35**, 500.
144 T. B. Huff, L. Tong, Y. Zhao, M. W. Hansen, J. J. Cheng and A. Wei, *Nanomedicine*, 2007, **2**, 125.
145 C. Loo, A. Lowery, N. Halas, J. West and R. Drezek, *Nano Lett.*, 2005, **5**, 709.
146 J. Chen, D. Wang, J. Xi, L. Au, A. Siekkinen, A. Warsen, Z.-Y. Li, H. Zhang, Y. Xia and X. Li, *Nano Lett.*, 2007, **7**, 1318.
147 C. J. Orendorff, S. C. Baxter, E. C. Goldsmith and C. J. Murphy, *Nanotechnology*, 2005, **16**, 2601.
148 J. W. Stone, P. N. Sisco, E. C. Goldsmith, S. C. Baxter and C. J. Murphy, *Nano Lett.*, 2007, **7**, 116.
149 J. D. Humphrey, *J. Biomech. Eng., Trans. ASME*, 2001, **123**, 638.
150 B. A. Roeder, K. Kokini, J. P. Robinson and S. L. Voytik-Harbin, *J. Biomech. Eng., Trans. ASME*, 2004, **126**, 699.
151 K. D. Costa, J. W. Holmes and A. D. McCulloch, *Philos. Trans. R. Soc. London, Ser. A*, 2001, **359**, 1233.
152 F. Grinnell, *Trends Cell Biol.*, 2003, **13**, 264.
153 D. E. Ingber, *Circ. Res.*, 2002, **91**, 877.
154 M. A. Swartz, D. J. Tshumperlin, R. D. Kamm and J. M. Drazen, *Proc. Natl. Acad. Sci. U. S. A.*, 2001, **98**, 6180.
155 G. Bao and S. Suresh, *Nat. Mater.*, 2003, **3**, 715.
156 C. Zhu, G. Bao and N. Wang, *Annu. Rev. Biomed. Eng.*, 2000, **2**, 189.
157 E. E. Connor, J. Mwamuka, A. Gole, C. J. Murphy and M. D. Wyatt, *Small*, 2005, **1**, 325.
158 K. Imura, T. Nagahara and H. Okamoto, *J. Am. Chem. Soc.*, 2004, **126**, 12730.
159 H. Wang, T. B. Huff, D. A. Zweifel, W. He, P. S. Low, A. Wei and J.-X. Cheng, *Proc. Natl. Acad. Sci. U. S. A.*, 2005, **102**, 15752.
160 N. J. Durr, T. Larson, D. K. Smith, B. A. Korgel, D. Sokolov and A. Ben-Yakar, *Nano Lett.*, 2007, **7**, 941.
161 M. Eghtedari, A. Oraevsky, J. Copland, N. Kotov, A. Conjusteau and M. Motamedi, *Nano Lett.*, 2007, **7**, 1914.